Sodium distribution in sodium tellurite glasses probed with spin-echo NMR

J. W. Zwanziger, J. C. McLaughlin, and S. L. Tagg
Department of Chemistry, Indiana University, Bloomington, Indiana 47405
(Received 21 February 1997)

We present results on the spatial distribution of sodium cations in sodium tellurite glasses as a function of sodium oxide content, obtained using a spin-echo NMR experiment. Glasses were studied with sodium oxide content ranging from 10 to 30 mol %. From the decay rate of the spin echo we infer the proximity of sodium nuclei at each composition. We found that at low sodium oxide contents the data are well modeled by a random distribution of sodium ions, with a closest approach distance of 3.2 Å in correspondence with sodium tellurite crystal structures. At higher sodium oxide contents, however, the data agree with sodium distributions that have extensive intermediate range order, on length scales of at least 10 Å. This ordering is most pronounced at 20% sodium oxide content, the composition at which this glass has been claimed to have maximum stability against devitrification. [S0163-1829(97)04233-1]

I. INTRODUCTION

While glasses form with no long-range atomic order, ordering on intermediate length scales is emerging as an important aspect of glass structure.[1–3] Here the length scale is divided into three regions: The short length scale extends over typical chemical bond distances, and reflects ordering due to covalent and ionic interactions; intermediate lengths extend to cover recurring aggregates of atoms, and can extend from several Å (small rings) to tens of Å; and the long length scale begins where the intermediate scale leaves off. Ordering in glasses on short length scales is common and well established, and merely indicates that the short-range forces in glasses are not significantly different from those in crystals. In particular, bond lengths in glasses deviate by at most a few percent from those in crystals; bond angles show greater variation, but typically 10% or less.

Glass structure at intermediate length scales reflects the propensity of the system to form extended aggregates, which nevertheless pack randomly and are themselves somewhat disordered. The size and types of these units may determine several bulk properties, including the ultimate limit of homogeneity of a given composition and its stability against devitrification.

The experimental detection and analysis of structural features on this length scale is quite challenging. Diffraction studies of glasses, using neutrons or x rays, often show features at low Q [the first sharp diffraction peak (FSDP)] that are interpreted as indicative of atomic clusters in real space.[3] The recent combination of x-ray- and neutron-weighted structure factors to analyze a single glass leads to much more insight into the origin of the FSDP, in particular, to which atomic correlations it is largely due.[1] Structural models, based on molecular dynamics or reverse Monte Carlo simulations, have also been constructed to probe the origin of intermediate-range order. In the case of phosphates, for example, the latter approach indicated that intermediate-range order arises from the extension of the phosphate chains,[4] while in silicates, molecular dynamics studies suggest clustering of the modifier ions.[2] Raman and NMR spectroscopies have been used to infer the existence of extended structural units in, for example, borate and chalcogenide glasses.

In this paper we present evidence for intermediate-length-scale ordering in tellurite glasses, obtained with a NMR experiment directly sensitive to through-space interactions. Whereas tellurite (TeO_2) is only a conditional glass former, requiring fast quenching from the melt to obtain glasses, alkali tellurites [$(M_2O)_x(TeO_2)_{1-x}$, M = Li, Na, K, Rb] have composition ranges of good glass formation that require only modest cooling rates. These glass families exhibit stability maxima, in that the difference between the crystallization temperature observed upon heating the glass and the glass transition temperature itself reaches a maximum as a function of composition.[5] In this sense certain compositions are most stable against devitrification. This behavior is shown for $(Na_2O)_x(TeO_2)_{1-x}$ glasses in Fig. 1. The stability maximum is achieved at about 20 mol % added Na_2O. Interestingly this system also displays a crystalline phase at this composition.[6,7]

The relationship between the glass structure at the atomic level and bulk properties, such as the stability against devitrification, is undoubtedly complex. In the case of $(Na_2O)_x(TeO_2)_{1-x}$ glasses the atomic structure undergoes substantial changes as a function of composition, beginning

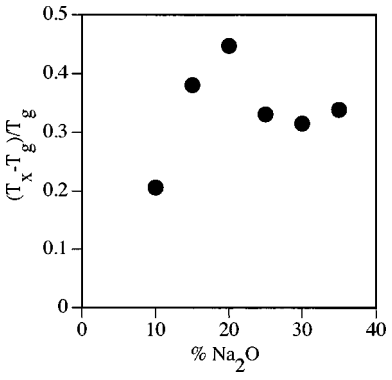

FIG. 1. Difference between crystallization temperature T_X (upon heating the glass) and glass transition temperature T_g, scaled to T_g for sodium tellurite glasses as a function of Na_2O content. After Ref. 5.

at about the 20 mol % composition. At this composition the coordination number of oxygen around the sodium cations begins to decrease, from nearly 6 at compositions less than 20 mol % to about 5 at the 35 mol % composition.[8] Moreover, the typical sodium environment at the 20 mol % composition differs substantially between the glass and the crystal, with the glass showing the *more* symmetric local environment. These findings indicate that, while the coordination of the sodium itself does not deviate markedly from typical behavior in solid oxides,[8,9] the glass structure as a function of composition begins to change substantially at the 20 mol % composition.

Changes in the glass structure have been suggested also in Raman[10,11] and diffraction[12] studies, which have focused on the tellurite network. As sodium oxide (or any modifier) is added, the network is cleaved, eventually resulting in TeO_3^{2-} ions at high modification levels. This process, as quantified by the appearance of nonbridging oxygen, has been inferred from vibrational spectroscopy and neutron-diffraction experiments. No dramatic changes near the 20 mol % composition were suggested, however.

In the present contribution we report experiments that measure the distribution of distances between pairs of sodium cations in $(Na_2O)_x(TeO_2)_{1-x}$ glasses. These measurements show evidence of substantial intermediate-range ordering in the sodium distribution at the 20 mol % composition. Compositions on both sides of this value show less ordering. We note that the 20 mol % composition coincides with the composition at which maximum stability against devitrification has been measured.[5]

II. EXPERIMENTAL METHODS

A. Sample preparation

$(Na_2O)_x(TeO_2)_{1-x}$ glasses were made by combining TeO_2 with Na_2CO_3, and heating to 800 °C for 15 min. By this time gas evolution had ceased. The liquids were quenched by pouring onto stainless steel. Electron microprobe analyses indicate that the final compositions are accurate to within two percentage points. The sodium-containing crystals (Table I) studied were purchased and used as received.

B. NMR experiments

The NMR experiment employed was a spin echo with variable dephasing time.[13–15] The pulse sequence is $(\pi/2)_x$-τ-$(\pi)_y$-acquire, that is, a preparation pulse, followed by a dephasing time τ, followed by a refocusing pulse. The resulting echo forms at time τ after the refocusing pulse. As discussed in more detail below, the echo amplitude decreases with increasing τ, due to magnetic dipole interactions that are not refocused by this pulse sequence. The rate of dephasing is quantified by the second moment M_2 [Eq. (2), below], which contains information about the distances between nuclei. The goal of the experiment is to measure and interpret M_2 as a function of glass composition.

The experiments were carried out on a home-built NMR spectrometer and an 8.46 T magnet, resulting in a ^{23}Na Larmor frequency of 95.2 MHz. The data presented were acquired at room temperature; to ensure that ion motion did not induce additional dephasing, selected glass samples were studied at 170 K. No differences between the dephasing behavior at the two temperatures were observed. Moreover, at 300 K in these samples, no sodium line narrowing or other evidence of significant ion motion is seen. This is in contrast to silicate glasses, where ion motion has been shown to affect this experiment.[14]

TABLE I. Experimental (M_{2E}) and calculated (M_{2C}) second moments, in units of 10^6 rad^2 sec^{-2}, for crystalline model compounds and sodium tellurite glasses.

Crystal	M_{2E}	M_{2C}	M_{2E}/M_{2C}
$NaClO_4$ (Ref. 22)	3.4	3.2	1.06
$NaNO_3$ (Ref. 23)	6.4	5.4	1.20
$Na_2C_2O_4$ (Ref. 24)	10.2	11.5	0.89
Na_2SO_4 (Ref. 25)	12.8	12.7	1.01
Na_2TeO_3 (Ref. 19)	9.2	13.3	0.70
Na_2SO_3 (Ref. 26)	12.8	16.0	0.80
Glass			
$(Na_2O)_{0.10}(TeO_2)_{0.90}$	0.90		
$(Na_2O)_{0.15}(TeO_2)_{0.85}$	1.3		
$(Na_2O)_{0.20}(TeO_2)_{0.80}$	5.5		
$(Na_2O)_{0.25}(TeO_2)_{0.75}$	5.8		
$(Na_2O)_{0.30}(TeO_2)_{0.70}$	6.7		

Moderate pulse powers were used, such that the $\pi/2$ pulse times were typically 5–7 μsec. This condition resulted in full excitation of the ^{23}Na central transition, with minimal coherence in the satellite transitions.[13,14] This is understood by realizing that the excitation bandwidth of a pulse is roughly $\nu_{rf}=1/t_{2\pi}$ Hz, where $t_{2\pi}$ is the duration of a resonant 2π pulse, while the linewidth of the central transition is $\Delta\nu$ (which includes chemical shift and second-order quadrupole effects, in addition to dipole couplings), and is known. The necessary pulse power is then given by the condition $\nu_{rf}/\Delta\nu \gtrsim 1$, because under this condition the central transition is completely excited, with little extra bandwidth available to excite the satellites. Note the dependence on pulse power, not the Fourier components due to the finite pulse length. To be sure, a small fraction of crystallites will be oriented such that their satellite transition frequencies lie within the excitation bandwidth, leading to a small but unavoidable systematic error. However, in the glasses studied here, the quadrupole coupling e^2Qq/h is of order 1.5–2 MHz, leading to a satellite spectral width of 0.75–1 MHz; our effective bandwidth was $\approx$36 kHz. Thus our bandwidth was at least a factor of 20 smaller than the satellite spectrum, leading to minimal contamination of the signal by the satellite transitions. To explore the pulse power dependence quantitatively we measured M_2 as a function of excitation bandwidth, for a crystalline sample of known M_2. The results show that the best results for M_2 are achieved at $\nu_{rf}/\Delta\nu \approx 2$–5.

A particularly important experimental detail was the use of small samples, typically 25% of the volume of the radio-frequency coil, and centered in the coil.[13] This geometry minimizes inhomogeneity effects at the ends of the coil, and was essential to the success of the experiments. The experi-

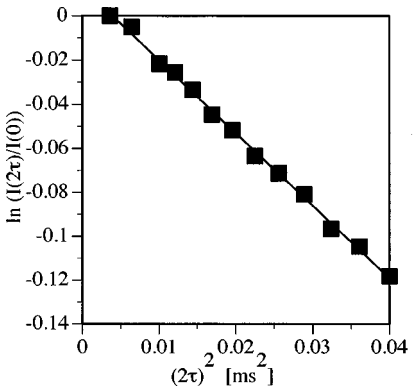

FIG. 2. Normalized spin-echo amplitudes, as a function of delay time, for sodium in $(Na_2O)_{20}(TeO_2)_{80}$ glass. The amplitudes are plotted on a logarithmic scale; the slope of the data is $-M_2/2$, where M_2 is the second moment of the resonance line.

ments were run multiple times on each sample, and on several samples of identical composition, to check reproducibility. The experimental precision judged from these runs was satisfactory, being on the order of 10%. The accuracy was determined by studying a range of sodium containing crystals with known structure. Here we found, especially for large M_2, that the data systematically underestimate the theoretical result, by typically 10%. This level of accuracy has been seen in other applications of this method,[14,15] and we take it into account in the interpretation of our data below.

III. RESULTS

Figures 2 and 3 show data from the spin-echo experiment, for one glass composition. The experiment was performed on $(Na_2O)_x(TeO_2)_{1-x}$ glasses of composition $x=0.10$–0.30. Data on selected compositions were also acquired at $-110\,^{\circ}C$. These data were indistinguishable from those at ambient temperature, indicating that ion mobility in $(Na_2O)_x(TeO_2)_{1-x}$ was negligible in its effect on the echo amplitudes. The same experiment was performed on a variety of sodium-containing crystalline salts, to use as checks of the accuracy and precision of the data. The second moments

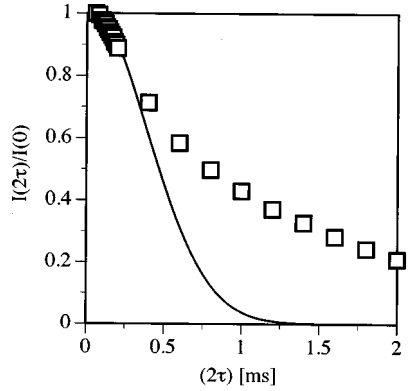

FIG. 3. Normalized spin-echo amplitudes, as a function of delay time, for sodium in $(Na_2O)_{20}(TeO_2)_{80}$ glass, plotted out to long refocusing times. Also shown is the Gaussian decay derived from the short-time data. Note the strong deviation from Gaussian behavior at longer refocusing times. This occurs because of the importance of higher moments to describe the dynamics.

extracted from this data are summarized in Table I, for the crystalline compounds and the sodium tellurite glasses.

IV. DISCUSSION

A. Theoretical foundation

Dipolar dephasing is well known as a probe of distance in solids as applied to spin-1/2 nuclei like phosphorus-31 and carbon-13; its use for quadrupolar nuclei (spin $I>1/2$) has been only recently developed and exploited.[13–15] The echo intensity decays with lengthening refocusing times due to the magnetic dipolar interactions between sodium nuclei. The dipole-dipole Hamiltonian is a perturbation with respect to the dominant Zeeman Hamiltonian, and so only the portion that commutes with the Zeeman Hamiltonian need be retained:[16]

$$H_D^0=\frac{1}{4}\gamma^2\hbar^2\sum_{j,k}\frac{1-3\cos^2\theta_{jk}}{r_{jk}^3}(3I_{jz}I_{kz}-\mathbf{I}_j\cdot\mathbf{I}_k). \qquad (1)$$

Here γ is the gyromagnetic ratio of ^{23}Na, j and k label different sodium nuclei, with spin $\mathbf{I}_j$ and $\mathbf{I}_k$, respectively, and separated by distance r_{jk}. θ_{jk} is the angle between the internuclear vector and the applied magnetic field, taken to be in the z direction. Because the dipole interaction is bilinear in the spin operators, it is not refocused by the pulse sequence. This happens essentially because *both* spin operators are flipped, leading to no change. In contrast, other interactions that are linear in $\mathbf{I}_j$, including chemical shift, heteronuclear dipole interactions, and the central transition subject to the second-order quadrupole effect, are refocused and thus have no effect on the echo amplitude.

The echo decay describes the resonance linewidth due solely to H_D^0, and can be simply approximated as the second moment of the resonance line. For short refocusing times the decay of the echo amplitude $I(2\tau)$ is dominated by the second moment, and hence has a Gaussian form

$$\frac{I(2\tau)}{I(0)}=\exp[-M_2(2\tau)^2/2]. \qquad (2)$$

The second moment M_2 follows from a second-order perturbation theory treatment of the evolution due to H_D^0. For a quadrupolar nucleus, the result depends on which transitions are being excited; Haase and Oldfield[13] have derived the expression

$$M_2=\frac{9}{4}E_L\gamma^4\hbar^2\sum_{j<k}\frac{(1-3\cos^2\theta_{j,k})^2}{r_{j,k}^6}, \qquad (3)$$

where the factor E_L incorporates matrix elements of the spin operators between the levels being excited. After averaging over all angles θ_{jk} and using constants appropriate to ^{23}Na, the resulting expression for the central transition is

$$M_2=2.66\times10^9\sum_{j<k}\frac{1}{r_{jk}^6}\mathrm{rad}^2/\mathrm{sec}^2. \qquad (4)$$

It is important to note here that Eq. (4) presumes selective excitation and detection of only the central transition, $|I=3/2,M=1/2\rangle\leftrightarrow|I=3/2,M=-1/2\rangle$, of the spin-3/2 nu-

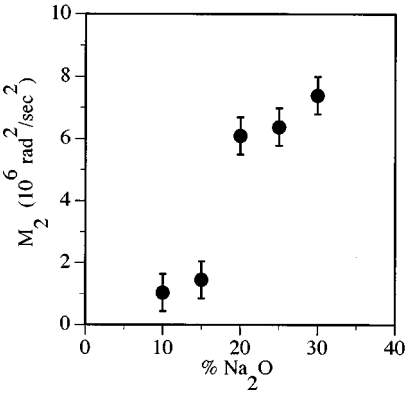

FIG. 4. M_2 as a function of composition in $(Na_2O)_x(TeO_2)_{1-x}$ glass. Two features should be noted: the overall monotonic increase and the sharp rise at the 20 mol % composition.

clei. This condition has been discussed in detail by Haase and Oldfield,[13] and is achievable when, as in the present case, the quadrupole interaction is large.

From the slopes of graphs of $\ln I(2\tau)/I(0)$ plotted as a function of $(2\tau)^2$ (Fig. 2), we extract M_2 and hence information about the distances between sodium nuclei in the glass. The resulting M_2 values for $(Na_2O)_x(TeO_2)_{1-x}$ glasses are shown in Fig. 4. The slopes were taken from the early portion of the decay curves, with $50 \lesssim \tau \lesssim 200$ μsec. This time corresponds to the first 10–25 % of the decay (less the initial few percent, Fig. 3), where the time scale is set by $M_2^{-1/2}$. At longer times, higher moments influence the dynamics, and plots like Fig. 2 deviate from linearity. The linearity of the data in this range shows that higher moments, which would induce dynamics like τ^4, etc., are not yet important. Another advantage of this mode of data analysis is that the data at very early times, which can be problematic to acquire with precision, are not needed.[14]

The information on intersodium distances contained in M_2 is not simple to interpret. While the form of Eq. (4) is explicit, it is only useful for crystals, for which all r_{jk} are known. For glasses it is convenient to rewrite Eq. (4) in terms of the sodium-sodium pair distribution function $g(r)$. This is done by replacing the sum in Eq. (4) with an integral, and realizing that the weight contributed at each distance r is given by the value of the sodium-sodium radial distribution function at that distance. Thus we have

$$M_2 \propto \sum_{j<k} \frac{1}{r_{jk}^6} \rightarrow \int \frac{4\pi r^2 \rho_0 g(r)}{r^6} dr, \tag{5}$$

where ρ_0 is the bulk number density of sodium and the integration is over the sample.

From Eq. (5) we see that M_2 yields $\langle r^{-6} \rangle$, where the averaging is carried out with respect to the sodium radial distribution function. Thus M_2 strongly emphasizes the correlations in the first few shells of atoms, with neighbors farther away contributing little. The experimental length scale can be estimated from Eq. (5), by approximating $g(r)$ by

$$\tilde{g}(r) = \begin{cases} 0 & r < R_0, \\ 1 & R_0 \leqslant r \leqslant R_s, \end{cases} \tag{6}$$

where R_0 is the closest approach of the sodium nuclei and R_s is the sample size. This simple estimate lets us evaluate M_2, and in particular the dependence of M_2 on the interaction length scale,

$$M_2(R) \propto \int_{R_0}^{R} \frac{4\pi r^2 \rho_0 g(r)}{r^6} dr. \tag{7}$$

Of particular interest is the ratio $M_2(R)/M_2(R_s)$, where R_s is the sample size ($R_s \gg R_0$). This ratio shows the length scale beyond which M_2 changes negligibly. Using Eq. (6) to solve $M_2(R)/M_2(R_s) = 0.95$ (that is, the value of R for which M_2 has reached 95% of its ultimate value) leads to $R \approx 20^{1/3} R_0$. Therefore, since $R_0 \approx 3$–4 Å for sodium oxides, this experiment yields information on correlations out to about 8–10 Å, or 2–3 coordination shells of sodium around sodium.

We also wish to point out that by formulating M_2 in terms of $g(r)$, the data from this type of experiment can be incorporated into modeling schemes such as reverse Monte Carlo algorithms.[17] While an integral of $g(r)$ is not nearly as sharp a constraint as $g(r)$ itself on a structural model, in many cases the alkali partial pair distribution function is not available anyway. In such cases M_2 data provide a useful model constraint to be used as a supplement to the total (neutron- or x-ray-weighted) pair distribution functions. We are currently attempting to use M_2 data in this way to model alkali tellurite glasses in real space.

B. Structural interpretation of the second moment

The utility of the present experiment has been demonstrated by Haase and Oldfield[13] and Gee and Eckert,[14] by comparing experimental M_2's obtained on crystalline samples to theoretical results based on evaluating Eq. (3). Our own comparison is contained in Table I, where it is seen that the accuracy is such that the experiment is useful for estimating qualitative trends, but not sufficiently high to discriminate between very similar structures. The table indicates that at low M_2 the experiment overestimates M_2, while at high M_2 the values obtained are low. However, note that the crystals used with low M_2 ($NaClO_3$ and $NaNO_3$) *also* have small values of ^{23}Na quadrupole coupling (<1 MHz), which increases the systematic error in this experiment. For the glass samples, the quadrupole couplings are larger (>1.5 MHz), similar to the crystals in Table I with high M_2's, though the glass M_2's are themselves on the low end of the range. Because of these various possible sources of systematic error, we used all the crystal calibration data uniformly, by fitting it to the linear relationship $M_{2C} = (1.1 \pm 0.1) M_{2E} - (0.2 \pm 0.8) \times 10^6$ rad^2 sec^{-2}. This fit indicates that the experimental values should be scaled by 1.1 before comparison with structures (we take the intercept to be zero). This factor is similar to that found in other applications.[14,15] In the following discussion we will always use this factor when comparing our data on glasses to model distributions.

A full model of the glass structure would include the sodium-sodium pair distribution function $g(r)$. Inverting the M_2 data to obtain it, however, is not possible in a unique way. To extract structural information from M_2 we must

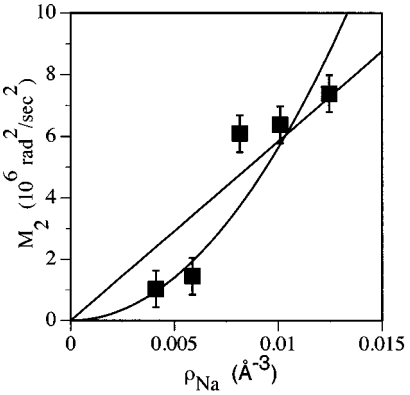

FIG. 5. M_2 data and fits to $M_2 \sim \rho^2$ and $M_2 \sim \rho$. The quadratic form is appropriate for isotropic dilation models of the sodium distribution, and the linear form for both decimated lattice and hard sphere distributions.

compare to plausible structural models, and look for general trends in M_2 as a function of composition.

Our measurements of M_2 show two gross qualitative features: a monotonic increase with increasing sodium content and a sharp rise near the 20 mol % composition. The monotonic increase is expected, since as the sodium content in the glass increases, the intersodium distance decreases. On the other hand, the remarkable rise at the 20 mol % composition is unexpected, and significantly exceeds the error limits imposed by the calibration. Thus there is a substantial change in the sodium ordering at this composition.

To interpret the data more fully, we compare the measured M_2's to those extracted from model distributions. We considered three types of models: sodium distributions extracted from isotropically dilating or compressing known sodium tellurite crystal structures, to obtain the correct sodium number density; random decimation of sodium tellurite lattices; and hard sphere distributions. All of these models produce monotonic increases in M_2 with increasing number density, though in different ways. The isotropically compressed models give $M_2 \sim r^{-6} \sim \rho^2$, because the number of interacting sodium is fixed, and only their distances are altered. The decimated lattice models show $M_2 \sim \rho$, because here the distance between sites is fixed, but the occupancy of each site is determined by ρ. Hard sphere distributions at the low densities appropriate here also show $M_2 \sim \rho$. Fits to the data of $M_2 \sim \rho^2$ and $M_2 \sim \rho$ are shown in Fig. 5. The figure shows that both types of models capture the monotonic increase, though neither fits the data in detail. This is because of the sharp increase at the 20% composition, which shows that the glass structure undergoes a qualitative change at and above this composition.

While the isotropic compression model captures the monotonic increase in M_2, it imposes other, unphysical constraints on the glass structure. In particular, it demands that all the bonds must be lengthened or compressed to achieve the correct glass density. It is well known that disorder in the bond lengths in glass is not a significant feature of their structures, with variations of no more than a few percent as compared to crystals. Therefore, we rejected the isotropic compression models as being unphysical.

The hard sphere model was constructed by considering the radial distribution function of a hard sphere liquid at the

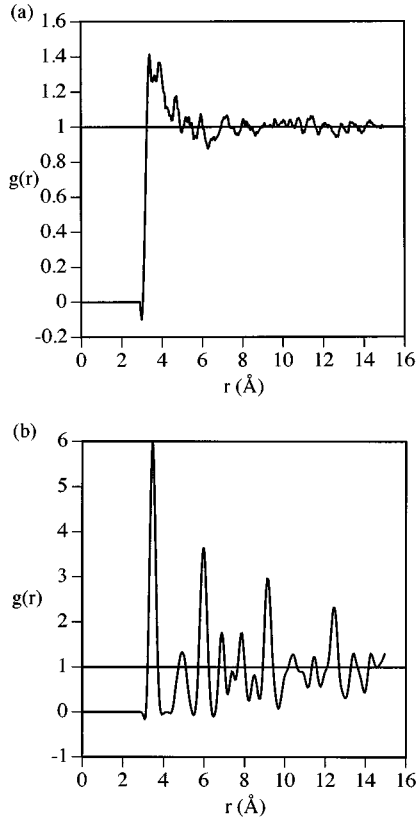

FIG. 6. Sodium pair distribution functions $g(r)$ for two model distributions: (a) the hard sphere model, with closest approach of 3.2 Å, and number density matching the $(Na_2O)_x(TeO_2)_{1-x}$ glass, with $x = 0.2$ (20 mol % Na_2O); (b) decimated lattice model based on the Na_2TeO_3 crystal structure, with sodium removed at random to achieve the number density of the glass with 20 mol % Na_2O.

same number density of each glass. Note that we do not mean to suggest that the sodium ions in tellurite glasses behave dynamically like a hard sphere liquid, but rather that as a first approximation their distribution in space can be modeled by the atomic distribution of a hard sphere liquid, at some particular instant in time. The hard sphere models were generated using 3.2 Å as the closest approach distance. This value was chosen based on the known sodium tellurite crystal structures [$Na_2Te_4O_9$ (Ref. 6), $Na_4Te_4O_{10}$ (Ref. 18), and Na_2TeO_3(Ref. 19)] for which the sodium ions never approach closer than this value. This is much larger than the ionic radius of sodium, of course, because the sodium cations are coordinated by oxygen and thus are always separated by at least one oxygen coordination shell, leading to the larger minimum distance. The resulting packing fractions for the hard sphere liquids were of order 0.1–0.2, far below the packing fraction at which a hard sphere liquid crystallizes.[20] An example of $g(r)$ constructed in this way for the 20 mol % Na_2O glass is shown in Fig. 6(a). From the $g(r)$ for each model, M_2 was calculated, using Eq. (5). These M_2 increase essentially linearly with sodium density over the range studied, much more like the glass data.

Decimated lattice models[14] were constructed by starting from the crystal structures of sodium tellurites with sodium densities higher than the target glasses. We made two such models, starting with $Na_4Te_4O_{10}$ (Ref. 18) and Na_2TeO_3 (Ref. 19). $Na_2Te_4O_9$ was not used, because it could not be

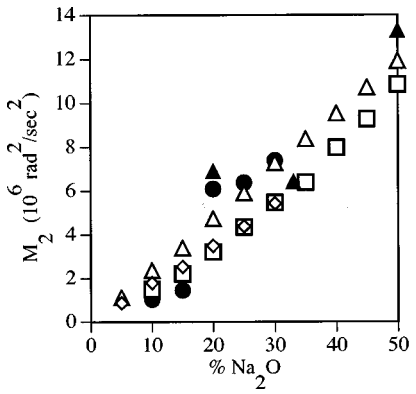

FIG. 7. M_2 values for the sodium tellurite glasses and different model distributions, as a function of sodium composition: □, hard sphere distribution at experimental sodium number density, with 3.2 Å closest approach; △, lattice model constructed by removing sodium at random from the crystal structure of Na_2TeO_3 until correct number density is achieved; ◇, same as △ but starting from $Na_4Te_4O_{10}$ crystal structure. ●, experimental M_2 values for $(Na_2O)_x(TeO_2)_{1-x}$ glasses; ▲, calculated M_2 values for crystalline sodium tellurites.

decimated and still cover the glass range investigated in this experiment. From the crystal structures used in the models, sodium ions were removed randomly until the number density corresponding to each glass composition was reached. The $g(r)$ of the resulting distribution was calculated, as was M_2 [Fig. 6(b) shows the $g(r)$ constructed in this way for the 20 mol % Na_2O glass based on the Na_2TeO_3 crystal structure]. The M_2 values again varied essentially linearly with density, as did the coordination number of sodium around sodium. The $g(r)$'s for the two classes of model are very different, however (Fig. 6). For the hard sphere model, $g(r) \approx 1$ for $r \gtrsim 8$ Å, while $g(r)$ for the decimated lattice models oscillates to some tens of Å, showing that the decimated lattice models are much more ordered. Figure 7 shows the M_2 values for the different models, overlaid with the experimental points. While all models capture the general trend of the data, and the magnitude, with no adjustable parameters, they fail to model the sharp increase in M_2 at the 20 mol % composition.

To make a detailed comparison between the data and the models, we subtract the model M_2 from the experimental M_2, and scale by the model value. These plots are shown in Fig. 8 for the three models. Figure 8(a) shows that at low sodium content the sodium ions are perhaps slightly farther apart on average than those in the hard sphere model, though given the error bars this difference may be insignificant. The differences at 20 mol % and above are significant, however, and show that a greater number of ions are found at close distances than in the hard sphere model. Taking the hard sphere model as the random reference system, we interpret this difference as a decrease in randomness, in other words the growth of order, at these compositions. The 20 mol % composition shows the greatest degree of sodium ordering in this sense.

In Figs. 8(b) and 8(c) we compare the experimental M_2 to the two decimated lattice models. Both models show a linear increase in M_2 with increasing sodium content, though with slightly different slopes. The difference in magnitude and

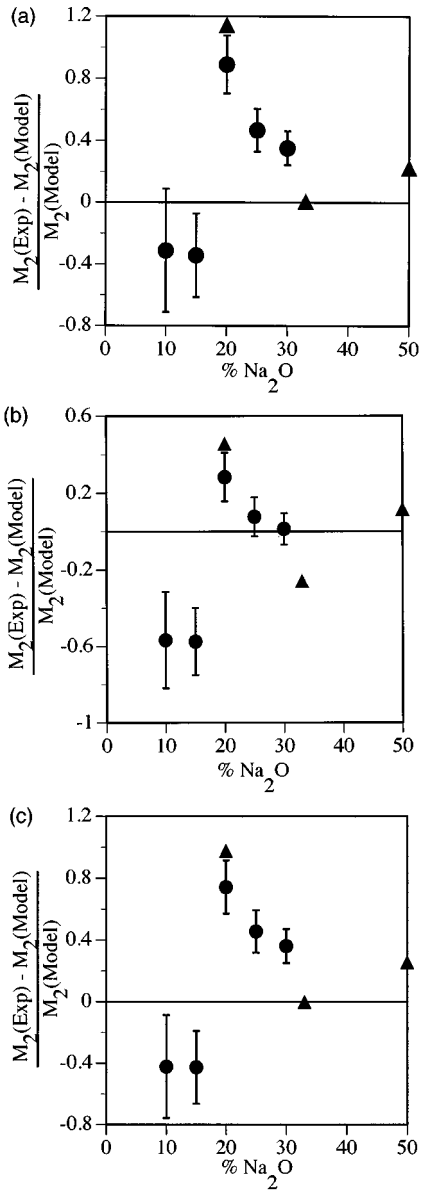

FIG. 8. Difference between experimental M_2 and model M_2, normalized to the model value, as a function of composition. This plot shows detailed deviations between the model and the data, after subtracting out the monotonic increase due to increasing sodium density. ●, experimental values for $(Na_2O)_x(TeO_2)_{1-x}$ glasses; ▲, calculated values for crystalline sodium tellurites. (a) Comparison with the hard sphere model; (b) comparison with the decimated lattice model based on Na_2TeO_3; (c) same as (b) but based on $Na_4Te_4O_{10}$. Note differences in vertical scale between (a), (b), and (c).

slope is a result of the different coordination numbers for each crystal: Na_2TeO_3 has a sodium-sodium coordination number of 7, while $Na_4Te_4O_{10}$ has a coordination number of 4. A higher coordination number means that a larger number of sodium ions remain around a given sodium ion at any concentration, resulting in a correspondingly larger M_2. The M_2 values for both decimated lattice models are larger at any given composition than M_2 from the hard sphere model; this is because the lattice models are much more ordered. At low sodium content, M_2 is lower for the glasses than for these models, indicating that the sodium ions are farther apart. At

20 mol % sodium the experimental M_2 is higher than those of the decimated lattice models, again indicating that the ions are in closer proximity in the glass than in these reference systems. At sodium content greater than 20 mol %, the second moment is significantly greater than that of the model based on $Na_4Te_4O_{10}$, while for the model based on Na_2TeO_3 the difference is within the error limits of the experiment. Figure 8(b) thus suggests that the local sodium ion packing in the glasses at higher compositions is similar to that in the decimated lattice model based on the Na_2TeO_3 crystal.

Thus, as judged by M_2, the sodium distribution at low sodium content is consistent with a hard sphere distribution, while at 20 mol % and above it is most consistent with that obtained from a decimated lattice based on Na_2TeO_3. The $g(r)$'s for these models (Fig. 6) show that the decimated lattice is much more ordered, but of particular importance is the small-r region where the present experiment is most sensitive. The amplitude of $g(r)$ in the two cases suggests that the structural change seen at 20 mol % may be one from well-separated, randomly placed cations (the hard sphere distribution) to clusters of cations [note the strong peak in $g(r)$ for the decimated lattice model at ≈ 3.5 Å].

V. CONCLUSIONS

The present experiment probes the spatial distribution of sodium in $(Na_2O)_x(TeO_2)_{1-x}$ glasses, as a function of composition. The basic quantity extracted is a weighted average of the sodium radial distribution function, specifically $\langle r^{-6} \rangle$. To interpret this in terms of distributions we compare to model systems, finding that both a random hard sphere distribution of sodium atoms with closest approach distance of 3.2 Å [as found in crystalline $(Na_2O)_x(TeO_2)_{1-x}$ phases] and decimated lattice models based on $Na_4Te_4O_{10}$ and Na_2TeO_3 capture the simplest aspects of the data. However, there appears to be a significant increase in cation proximity near the 20 mol % composition, as compared to a random distribution. Moreover, we have previously shown that the individual sodium sites in the 20 mol % glass are markedly different from those of the $Na_2Te_4O_9$ crystal.[8] That earlier result combined with the present measurements indicates that the elements of the glass structure due to the cations differ significantly from the crystal, both in the geometry of the cation coordination sites and in their spatial distribution. This difference is most marked at the 20 mol % composition, which coincides with the composition of maximum glass stability.[5] Our conclusion is that, because the structure of crystal and glass differ so substantially at this composition, the glass is especially stable against crystallization on heating, since evidently it would have to undergo too large a structural rearrangement given the amount of thermal energy available.

The ordering of the sodium is not immediately apparent in the structure factors obtained from neutron diffraction, because the Na-Na partial contribution to the total structure factor is small.[21] For example, the first sharp diffraction peak does not scale in amplitude or location with sodium content. We are analyzing our neutron-diffraction data more fully, to combine information on the tellurite network with the present results, and hopefully quantify the above conjecture on the difference between the glass and crystal structures.

ACKNOWLEDGMENT

This research was supported by the National Science Foundation, Grant No. DMR-9508625.

[1] P. Armand *et al.*, Europhys. Lett. **29**, 549 (1995).
[2] G. N. Greaves *et al.*, Philos. Mag. A **64**, 1059 (1991).
[3] S. R. Elliott, Nature (London) **354**, 445 (1991).
[4] J. D. Wicks *et al.*, Phys. Rev. Lett. **74**, 726 (1995).
[5] J. Heo *et al.*, J. Am. Ceram. Soc. **75**, 277 (1992).
[6] S. L. Tagg, J. C. Huffman, and J. W. Zwanziger, Chem. Mater. **6**, 1884 (1994).
[7] *Tellur, Gmelin Handbuch der Anorganischen Chemie*, edited by G. Hantke (Springer-Verlag, Berlin, 1976).
[8] S. L. Tagg, R. E. Youngman, and J. W. Zwanziger, J. Phys. Chem. **99**, 5111 (1995).
[9] J. W. Zwanziger, S. L. Tagg, and J. C. Huffman, Science **268**, 1510 (1995).
[10] T. Sekiya, N. Mochida, A. Ohtsuka, and M. Tonokawa, J. Non-Cryst. Solids **144**, 128 (1992).
[11] M. Tatsumisago, T. Minami, Y. Kowada, and H. Adachi, Phys. Chem. Glasses **35**, 89 (1994).
[12] S. Neov *et al.*, J. Phys. C **12**, 2475 (1979).
[13] J. Haase and E. Oldfield, J. Magn. Reson. Ser. A **101**, 30 (1993).
[14] B. Gee and H. Eckert, Solid State NMR **5**, 113 (1995).
[15] A. T.-W. Yap, H. Förster, and S. R. Elliott, Phys. Rev. Lett. **75**, 3946 (1995).
[16] C. P. Slichter, *Principles of Magnetic Resonance*, 3rd ed. (Springer, New York, 1989).
[17] R. L. McGreevy and M. A. Howe, Annu. Rev. Mater. Sci. **22**, 217 (1992).
[18] S. L. Tagg, J. C. Huffman, and J. W. Zwanziger, Acta Chem. Scand. **51**, 118 (1997).
[19] R. Masse, J. C. Guitel, and I. Tordjman, Mater. Res. Bull. **15**, 431 (1980).
[20] P. M. Chaiken and T. C. Lubensky, *Principles of Condensed Matter Physics* (Cambridge University Press, Cambridge, England, 1995).
[21] S. L. Tagg and J. W. Zwanziger (unpublished).
[22] V. R. Wartchow and H. J. Berthold, Z. Kristallogr. **147**, 307 (1987).
[23] V. S. Göttlicher and C. D. Knöchel, Acta Crystallogr. Sect. B **36**, 1271 (1980).
[24] D. A. Reed and M. M. Almstead, Acta Crystallogr. Sect. B **37**, 938 (1981).
[25] A. G. Nord, Acta Chem. Scand. **27**, 814 (1973).
[26] L. O. Larsson and P. Kierkegaard, Acta Chem. Scand. **23**, 2253 (1969).